CrossMark

An assessment of upper ocean salinity content from the Ocean Reanalyses Inter-comparison Project (ORA-IP)

L. Shi[1] · O. Alves[1] · R. Wedd[1] · M. A. Balmaseda[2] · Y. Chang[3,16] · G. Chepurin[4] ·
N. Ferry[10] · Y. Fujii[5] · F. Gaillard[6] · S. A. Good[7] · S. Guinehut[8] · K. Haines[9] ·
F. Hernandez[10,17] · T. Lee[11] · M. Palmer[7] · K.A. Peterson[7] · S. Masuda[12] · A. Storto[13] ·
T. Toyoda[5] · M. Valdivieso[9] · G. Vernieres[14] · X. Wang[15] · Y. Yin[1]

Abstract Many institutions worldwide have developed ocean reanalyses systems (ORAs) utilizing a variety of ocean models and assimilation techniques. However, the quality of salinity reanalyses arising from the various ORAs has not yet been comprehensively assessed. In this study, we assess the upper ocean salinity content (depth-averaged over 0–700 m) from 14 ORAs and 3 objective ocean analysis systems (OOAs) as part of the Ocean Reanalyses Intercomparison Project. Our results show that the best agreement between estimates of salinity from different ORAs is obtained in the tropical Pacific, likely due to relatively abundant atmospheric and oceanic observations in this region. The largest disagreement in salinity reanalyses is in the Southern Ocean along the Antarctic circumpolar current as a consequence of the sparseness of both atmospheric and oceanic observations in this region. The West Pacific warm pool is the largest region where the signal to noise ratio of reanalysed salinity anomalies is >1. Therefore, the current salinity reanalyses in the tropical Pacific Ocean may be more reliable than those in the Southern Ocean and regions along the western boundary currents. Moreover, we found that the assimilation of salinity in ocean regions with relatively strong ocean fronts is still a common problem as seen in most ORAs. The impact of the Argo data on the salinity reanalyses is visible, especially

This paper is a contribution to the special issue on Ocean estimation from an ensemble of global ocean reanalyses, consisting of papers from the Ocean Reanalyses Intercomparison Project (ORAIP), coordinated by CLIVAR-GSOP and GODAE OceanView. The special issue also contains specific studies using single reanalysis systems.

✉ L. Shi
l.shi@bom.gov.au

[1] Research and Development Branch, Bureau of Meteorology, Melbourne, VIC, Australia

[2] European Centre for Medium-Range Weather Forecasting (ECMWF), Reading, UK

[3] Geophysical Fluid Dynamics Laboratory (GFDL), Princeton University, Princeton, NJ, USA

[4] University of Maryland, College Park, MD, USA

[5] Meteorological Research Institute (MRI), Japan Meteorological Agency, Tsukuba, Japan

[6] Ifremer, UMR 6523, LPO, CNRS/Ifremer/IRD/UBO, CS 10070, 29280 Plouzane, France

[7] Met Office Hadley Centre, Exeter, UK

[8] Collecte Localisation Satellites (CLS), Ramonville Saint-Agne, France

[9] NCEO, Reading University, Reading, UK

[10] Mercator Océan, Ramonville Saint Agne, France

[11] Jet Propulsion Laboratory (JPL), California Institute of Technology, Pasadena, California, USA

[12] Research and Development Center for Global Change, Japan Agency for Marine-Earth Science and Technology, Yokosuka, Japan

[13] Euro-Mediterranean Centre for Climate Change (CMCC), Bologna, Italy

[14] Global Modeling and Assimilation Office (GMAO), NASA, Washington, DC, USA

[15] Joint Institute for Regional Earth System Science and Engineering (JIFRESSE), UCLA, Los Angeles, CA, USA

[16] Department of Earth Science, Kongju National University, Gongju, Korea

[17] Institut de Recherche pour le Développement (IRD), Toulouse, France

within the upper 500 m, where the interannual variability is large. The increasing trend in global-averaged salinity anomalies can only be found within the top 0–300 m layer, but with quite large diversity among different ORAs. Beneath the 300 m depth, the global-averaged salinity anomalies from most ORAs switch their trends from a slightly growing trend before 2002 to a decreasing trend after 2002. The rapid switch in the trend is most likely an artefact of the dramatic change in the observing system due to the implementation of Argo.

1 Introduction

Studies of the seasonal variability of salinity in the tropical oceans have revealed that the salinity changes, in particular in the upper ocean, are strongly impacted by river discharges, surface freshwater flux (i.e., evaporation and precipitation; referred as E–P hereafter), and advection etc. (Cronin and McPhaden 1998; Johnson et al. 2002; Foltz et al. 2004). On decadal timescales, changes in global ocean salinity can be mainly attributed to changes in the global hydrological cycle, in particular the E–P pattern changes, (Curry et al. 2003; Durack and Wijffels 2010; Durack et al. 2012) that is possibly linked to global warming (Held and Soden 2006). In the high latitude Atlantic, the long-term salinity changes are impacted by the wind-driven export of ice, river discharge from the Arctic and advection by the currents (Vinje 2001; Belkin 2004).

A number of papers have indicated that salinity has a great impact on the global ocean dynamical and thermal circulation through density and dynamical height variations (Cooper 1988; Rahmstorf 1996; Murtugudde and Busalacchi 1998; Vialard et al. 2002; Fedorov et al. 2004; Zhang and Vallis 2006; Huang et al. 2008). For instance, "Great Salinity Anomalies (GSAs)" events, that have occurred during the 1970s, 1980s and 1990s in the North Atlantic Ocean (Dickson et al. 1988; Belkin et al. 1998; Belkin 2004), may play an important role in the variations of the thermohaline circulation, deep western boundary current, northern recirculation gyre, and Gulf Stream, etc. (Wadley and Bigg 2006; Zhang and Vallis 2006). The close link between salinity variability in the western Pacific and subsequent ENSO events has also been revealed from both observational investigations and dynamical model simulations (Maes et al. 2005, 2006; O'Kane et al. 2014; Zhu et al. 2014). Furthermore, some studies have pointed out that the assimilation of observed salinity can provide more accurate initial ocean states for dynamical models since the imbalance between temperature and salinity is reduced, thereby

resulting in better ENSO prediction skills (Ballabrera-Poy et al. 2002; Vialard et al. 2002; Yang et al. 2010; Hackert et al. 2011; Zhao et al. 2013, 2014; Zhu et al. 2014).

Most research and operational centres around the world have established their own ocean reanalysis systems (ORAs) for the purpose of building up historical ocean datasets and providing initial conditions for a range of forecast systems. In the early stages, the products from ORAs (Balmaseda et al. 2009) mainly focused on the assimilation of observed temperature, while salinity was not adjusted at all or was constructed from the local climatological temperature–salinity (T–S) relationship, mainly due to the paucity of salinity observations (Behringer and Xue 2004). Since the international Argo Project (http://argo.jcommops.org), which collects real-time temperature and salinity profiles in upper 2000 metres of the ocean, started to provide comprehensive global ocean coverage from around 2006 onwards, most state-of-the-art ORAs assimilate both observed sea temperature and salinity profiles by using a variety of assimilation methods (Table 1).

To date, there is no intercomparison of the performance of salinity reanalyses from the latest vintage of ORAs from around the world. However, there have been several assessments of salinity analyses from some individual ORAs (Hernandez et al. 2009; Xue et al. 2011; Chang et al. 2012; Fujii et al. 2012). The Ocean Reanalyses Intercomparison Project (ORA-IP) was proposed by the participants of the joint GODAE (Global Ocean Data Assimilation Experiment) OceanView/CLIVAR GSOP (Global Synthesis and Observation Panel) workshop in Santa Cruz in June 2011 for the purpose of real time ocean monitoring and operational seasonal forecast systems improvement (Balmaseda et al. 2015). The work presented here is a contribution to the ORA-IP project. Its primary objective is to quantify the ensemble spread and signal to noise ratio in the estimation of salinity from an ensemble of existing global ocean reanalyses. This is the first step to evaluate the maturity level of existing global products. By identifying current deficiencies, it is expected that ORA-IP can help with the future development of ocean data assimilation and observing systems. The work presented here is only an initial and broad quantification of the signal to noise ratio, and it will not deal with the representation of process or specific modes of variability. We expect that further studies can follow once the ORA-IP data is made publicly available.

This paper is organized into six sections. Section 2 presents a brief description of the ORAs included in this study. The mean state of the reanalysed salinity for the period from 1993 to 2010[1] is assessed in Sect. 3. In Sect. 4, the variability

---

[1] Exception is the ISAS13, which is only available from 2002 to 2010 in this study. Hereafter, all the calculation of ISAS13, thus, is based on the period from 2002 to 2010.

Table 1 List of the ocean data assimilation systems

Products	Ocean models	Forcing	Main Assim. method	Data assimilated	Relax to clim.
ECCOV4[a] (MIT/AER/JPL)	MITGCM 1° × (0.4°–1.0°); 50 vertical levels	ERAi + CORE Bulk	4DVAR Adjoint	T/S; SLA; SSH; SST	None
GMAO[b] (GSFC/NASA)	MOM4p1 0.5°; 40 vertical levels	MERRA + Bulk	EnOI	T/S; SST;	SSS
SODA[c] (Uni. Maryland and TAMU)	POP2.1 0.25° × 0.4°; 40 vertical levels	ERA40 and ERAi (since 2002) + Bulk	OI	T/S; SST	SSS (3 months); 3D T/S (10 years)
GloSea5[d] (Met Office, UK)	NEMO3.2 1/4°; 75 vertical levels	ERAi + CORE Bulk	3DVAR	T/S; SST; SLA; SIC	Surface Haney restoring + 3D T/S (360 days)
ORAS3[e] (ECMWF)	HOPE 1° × (0.3°–1°); 29 vertical levels	ERA40 and ECMWF operational analysis (since 2002)	OI	T/S; SST; SLA	SSS (3 years); 3D T/S (10 years)
ORAS4[f] (ECMWF)	NEMO3.0 1° × 1°; 42 vertical levels	ERA40 to 1988, ERAi thereafter + Flux	3DVAR	T/S; SST; SLA	SSS (1 year); 3D T/S (20 years)
CGLORS[g] (CMCC/IT)	NEMO3.2.1-LIM2 0.5° × 0.5°; 50 vertical levels	ERAi + CORE Bulk	3DVAR	T/S; SLA; SST; SIC	SSS (300 days); 3D T/S
PEODAS[h] (BOM/AUS)	MOM2 2° × (0.5°–1.5°); 25 vertical levels	ERA40 and NCEP2 (since 2002)	EnKF	T/S; SST	SSS (1 year); 3D T/S (2 years)
PECDAS (BOM/AUS)	MOM2 2° × (0.5°–1.5°); 25 vertical levels	Atmospheric component of the coupled model	EnKF	T/S; SST	SSS (1 year); 3D T/S (2 years)
ECDA[i] (GFDL/NOAA)	CM2.1/MOM4 1° × (0.3°–1°); 50 vertical levels	Atmospheric component of the coupled model	EnKF	T/S; SST	None
MOVE-C[j] (MRI/JMA)	MRI.COM V2 1° × (0.3°–1.0°); 50 vertical levels	Atmospheric component of the coupled model	MOVE 3DVAR-IAU	T/S; SSH; SST	SSS (10 days); 3D T/S (5 years)
MOVE-G2[k] (MRI/JMA)	MRI.COM V3 1° × (0.3°–0.5°); 52 vertical levels	JRA-55 CORE Bulk	MOVE 3DVAR-FGAT-IAU	T/S; SSH; SST	3D T/S (5 years)
K7ODA[l] (ESTOC) (JAMSTEC/RCGC)	MOM3-based OGCM 1° × 1°; 45 vertical levels	NCEP-R1 + Corr. Flux	4DVAR Adjoint	T/S; SLA; SST	BC(30 days by IAU)
G2V3 (Mercator Océan/FR)	NEMO3.1-LIM2evp 1/4°; 75 vertical levels	ERAi Corr + CORE Bulk	SAM2V1—SEEK filter + 3DVAR	T/S; SLA; SST; SIC	3D T/S (360 days)
ARMOR3D[m] (CLS/FR)	No model 1/3°; 24 vertical levels	N/A	Objective analysis	T/S; SLA; SST	None
ISAS13 (LPO/Ifremer)	No model 0.5°; 152 vertical levels	N/A	Objective analysis	T/S	None
EN3v2a[n] (Met Office, UK)	No model 1° × 1°; 42 vertical levels	N/A	Objective analysis	T/S	None

T/S Temperature/salinity profiles, *SSH* sea surface height from tide gauges, *SLA* altimeter-derived sea level anomalies from satellite observation, *SIC* satellite derived sea ice concentration, *BC* lateral boundary conditions, *IAU* incremental analysis updates

[a] Marshall et al. (1997), [b] Vernieres et al. (2012), [c] Carton and Giese (2008), [d] Waters et al. (2014), [e] Balmaseda et al. (2008), [f] Balmaseda et al. (2013), [g] Storto et al. (2011), [h] Yin et al. (2011), [i] Zhang et al. (2007), [j] Fujii et al. (2009), [k] Toyoda et al. (2013), [l] Masuda et al. (2010), [m] Guinehut et al. (2012), [n] Ingleby and Huddleston (2007)

of the salinity reanalyses, such as standard deviation, signal-to-noise ratio and temporal correlation is evaluated. In this section, the temporal correlation between local salinity anomalies and temperature anomalies and the impact of Argo data on the salinity reanalyses is also discussed. Furthermore, we will also examine the trend in global average salinity anomalies over depth levels above 1500 m in Sect. 5. The final section contains a discussion and conclusions.

2 Reanalyses systems

Critical information (e.g., referred names and associated institutions; ocean model resolutions; atmospheric forcing; main assimilation methods, assimilated observations and relaxation to climatology) of the products assessed in this study is summarized in Table 1. The total of 17 estimates can be roughly classified into two groups: the first one consists of fourteen ORAs (the first fourteen in Table 1) which all assimilated various ocean observations into a variety of dynamical ocean model systems (coupled or uncoupled); the second group, in contrast, consists of ARMOR3D, ISAS13 and EN3v2a in which their salinity reanalyses are obtained from ocean observations through a statistical method with no dynamical ocean model. Thus, the three products in the second group are referred to as Objective Ocean Analyses (OOAs) hereafter.

The main assimilation techniques used by the fourteen ORAs can be simply summarised as: Optimal Interpolation (OI; e.g., SODA and ORAS3), Ensemble OI (EnOI; e.g., GMAO), 3-dimension variational method (3DVAR; e.g., GloSea5, ORAS4, CGLORS, MOVE-C, MOVE-G2 and G2V3), 4-dimension variational method (4DVAR; e.g., ECCOV4 and K7ODA[2]), Kalman Filter method (KF; e.g., G2V3), and Ensemble Kalman Filter (EnKF; e.g., ECDA, PEODAS,[3] PECDAS). The atmospheric surface forcing for most of the 14 ORAs are obtained from atmospheric reanalyses through a variety of methodologies (e.g., corrected fluxes, different bulk formulations) except that three ORAs (e.g., PECDAS, ECDA and MOVE-C) are provided by the atmospheric component of the corresponding coupled model.

In addition to observed Temperature/Salinity (T/S) profiles, various other ocean observations, such as altimeter-derived Seal Level Anomalies (SLA); Sea Surface Height (SSH) from tide gauges; Sea Surface Temperature (SST) and satellite derived Sea-Ice Concentration (SIC), are also assimilated by some of the ORAs in Table 1. In order to

prevent the model from drifting, most ORAs relax their 3 dimensional (3D) T/S or Sea Surface Salinity (SSS) to climatology with differing relaxation time intervals (Table 1). Although a few studies have suggested the potential impact of SSS on SST variability in the tropical Pacific (Ballabrera-Poy et al. 2002; Wang and Chao 2004; Hackert et al. 2011), the performance of SSS reanalyses will not be assessed in this paper because SSS is defined differently in each ORA (e.g., different layer depths). In this study, we will mainly focus on the depth-averaged salinity over the upper 0–700 m ocean layer[4] (S700) since the largest salinity changes are usually observed in the upper 500 m (Curry et al. 2003; Boyer et al. 2005; Durack and Wijffels 2010). For this study, all the monthly salinity fields from the ORA-IP participants have been interpolated to a standard $1° \times 1°$ latitude-longitude grid.

The biggest problem in the assessment of salinity reanalyses from various ORAs is the absence of "reality" or proper standard due to the paucity of salinity observations, especially prior to Argo. We will focus on the ensemble spread (SPD; refer to the Eqs. (2, 3) for details; noted as ensemble standard deviation in Balmaseda et al. 2015) of the variable 'X' from 14 ORAs about their corresponding ensemble mean (EMORA; refer to the Eq. (1) for details). This can be used to measure the diversity/agreement of the salinity between different ORAs. Following previous studies (Lee et al. 2009; Zhu et al. 2012), we also consider the standard deviation (STD; refer to STD_{EMORA}^{A} in the Eq. (8)) of EMORA variability as the 'signal' (or certainty) part of the variability of salinity reanalyses from the 14 ORAs. Thus, the corresponding SPD (refer to SPD_{EMORA}^{X} in the Eqs. (2, 3)) can be considered a quantitive measurement of the 'noise' (or uncertainty), which is caused by different assimilation methods, atmospheric forcing and ocean model dynamics etc., from the 14 ORAs. Therefore, the 'uncertainty' mentioned hereafter in this study cannot simply be considered as the true 'error' between the reanalyses and the observations. For instance, it is possible that all the products have similar systematic error, which will not be captured by this ensemble method. As discussed by Balmaseda et al. (2015), the ensemble method also assumes that all the estimates have similar quality, which may not always be applicable.

The ensemble mean of the 3 OOAs [EMOO; refer to $\overline{X_{EMOO}}$ or X_{EMOO}^{A} in the Eq. (1)] will be compared with EMORA in this paper. This comparison should illustrate the main differences between statistical and dynamical data assimilation estimates, assuming the bulk of in situ salinity

---

[2] Changes in water volume in conjunction with a free surface model used by K7ODA are ignored in this study.

[3] In a strict sense, PEODAS is an approximate form of an ensemble Kalman filter system (Yin et al. 2011).

[4] The S700 values in the ocean coast regions, where the deepest depth is less than 700 m, are defined as missing value.

observations are likely to be similar in ORAs and OOAs. The salinity from OOAs is likely to be close to climatology prior to Argo due to the lack of observations. Even during the Argo period, we note that the salinity reanalyses from the 3 OOAs or the corresponding EMOO cannot simply be considered as the proxy of 'reality' due to inhomogeneous temporal and spatial distribution of Argo. In contrast, the salinity in ORAs is affected not only by the salinity observations, but also by model dynamics and mixing, surface fluxes, and imposed multivariate relations (for instance, observations of temperature and sea level can affect the salinity). This variety of information sources in ORAs can contribute to the coherence of the signal, but also to the ensemble spread, since there is large uncertainty in ocean models, surface fluxes and multivariate relationships.

3 Mean state

Compared to EMOO (Fig. 1b), the AMS700 of EMORA (Fig. 1a) is relatively saltier (≥ 0.1 psu) in the Southern Ocean along the Antarctic Circumpolar Current (ACC) and in the Kuroshio. A striking dipole appears along the Gulf Stream/Labrador Current system, where the AMS700 of EMORA is fresher/saltier than that of EMOO by more than 0.1 psu, respectively. This difference is consistent with the well-known systematic error in ocean models (incorrect strength and path of the Gulf Stream and Labrador Current). It is likely that in this area EMOO are relatively well constrained by the existing salinity observations. The large differences along the northern edge of the ACC are also likely to have a dynamical origin, but in this case EMOO may have significant uncertainty, due the paucity of in situ observations. There are also large scale differences in the meridional distribution of salinity, which varies across basins. Thus, in the Atlantic, the AMS700 of EMORA shows a saltier equatorial band and fresher sub-tropical gyres than that of EMOO, while the opposite pattern occurs in the Pacific. Differences associated with the Equatorial Pacific current system are also visible.

Generally, the regions of relatively large SPD_{EMORA}^{AM} of AMS700 ($SPD_{EMORA}^{AM} \geq 0.1$ psu) shown in Fig. 1c, such as in the Southern Ocean along the ACC, the Kuroshio and the Gulf Stream, correspond with the regions of relatively large differences of AMS700 shown in Fig. 1a. This indicates that the existing observations are not able to constrain the large diversity among different ORAs in these areas, at least with the current assimilation systems. The spatial pattern of SPD_{EMORA}^{AM} in the Atlantic resembles the footprint of the wind driven circulation.

In order to demonstrate the individual performance of each ORA, the zonal distributions of the differences of AMS700 between each product and EMOO are shown
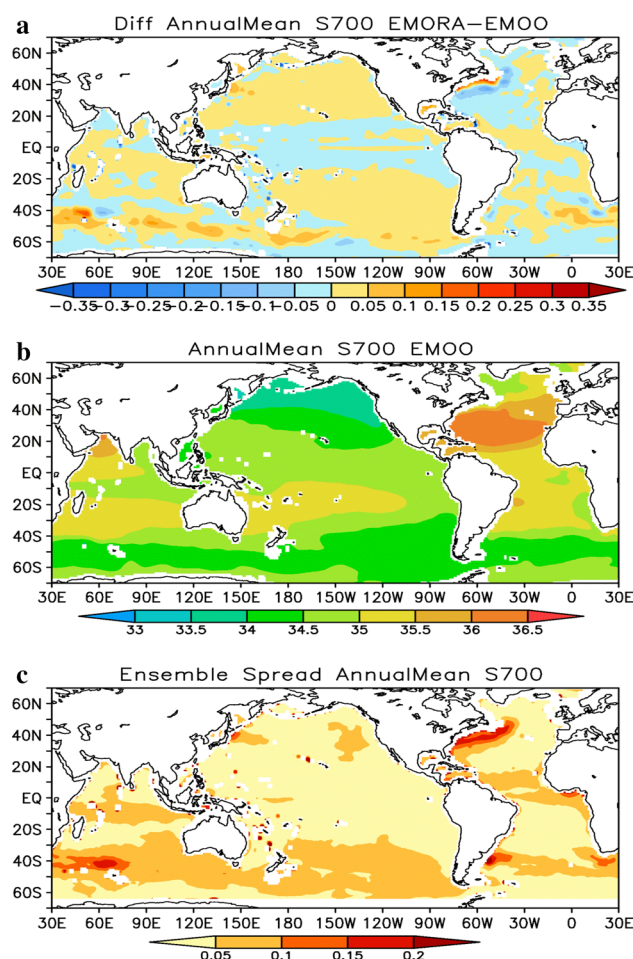

Fig. 1 **a** Differences of the annual mean S700 (AMS700) between the ensemble mean of ORAs (EMORA) and the ensemble mean of 3 OOAs (EMOO) for the period 1993–2010. **b** The distribution of AMS700 from EMOO for the period 1993–2010. **c** The ensemble spread (i.e. SPD_{EMORA}^{AM}) of AMS700 from individual ORAs about the corresponding EMORA. The unit of *colour bar* is psu

in Fig. 2a (meridionally averaged over 30°N–60°N), b (15°S–15°N) and c (60°S–30°S), respectively. The definition of the shaded band in Fig. 2, which represents the uncertainty range (i.e., UCR_{EMORA}^{AM}) of AMS700 differences from the 14 ORAs about their EMORA, is detailed in the Eq. (4). Thus, the ORAs outside the shaded band can be considered as outliers.

The AMS700 differences between OOAs and EMOO are generally smaller than that between each ORA and EMOO in most parts of oceans except for the relatively large AMS700 differences for ISAS13 shown in the northern Atlantic and the tropical Pacific. This feature can probably be attributed to the calculation period for the ISAS13 (i.e., 2002–2010) which is shorter than that for other products (i.e., 1993–2010).

In the northern band (averaged over 30°N–60°N; Fig. 2a), the *UCR* of AMS700 differences gradually
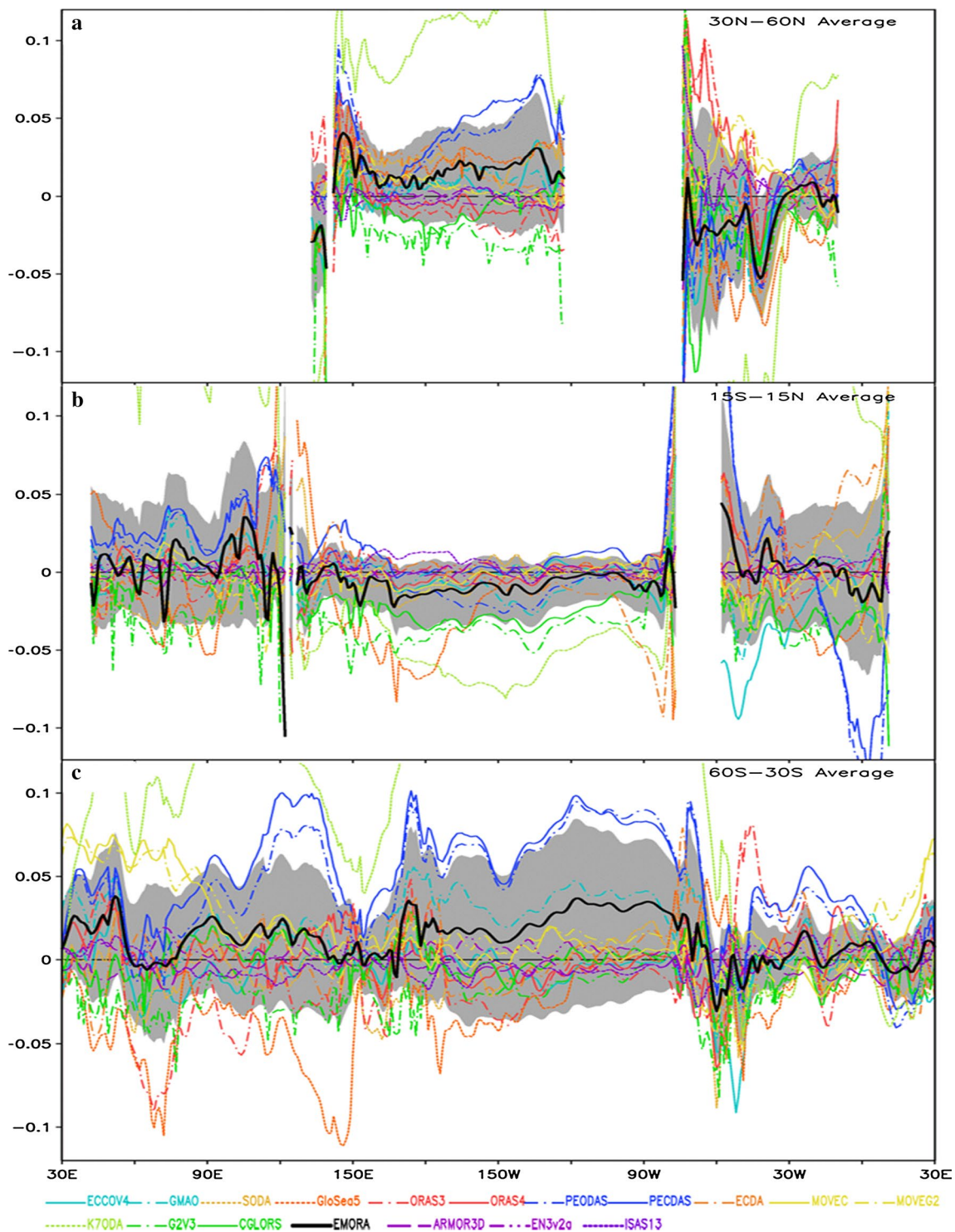
Fig. 2 **a** Zonal distributions of differences of meridionally-averaged (over 30°N–60°N) AMS700 between individual reanalysis systems and EMOO for the period 1993–2010. The definition of *shaded band* (i.e. UCR_{EMORA}^{AM}) can be referred to the Eq. (4). **b** Same as in **a**, except for meridionally-averaged over 15°S–15°N. **c** Same as in **a**, except for meridionally-averaged over 60°S–30°S. The unit of ordinate is psu

increases eastward in the northern Pacific Ocean, but gradually decreases eastwards in the North Atlantic Ocean. Compared to the tropical Indian Ocean and Atlantic Ocean, the obviously smaller *UCR* of AMS700 differences in the tropical Pacific Ocean can be attributed to the relative abundance of observations there. The *UCR* of AMS700

Fig. 3 Differences of the seasonal cycle (i.e. monthly climatology for the period 1999–2010) S700 between all products and the TAO/TRITON data at 8°N156°E. The definition of *shaded band* (i.e. UCR_{EMORA}^{SC}) can be referred to the Eq. (4). The unit of ordinate is psu
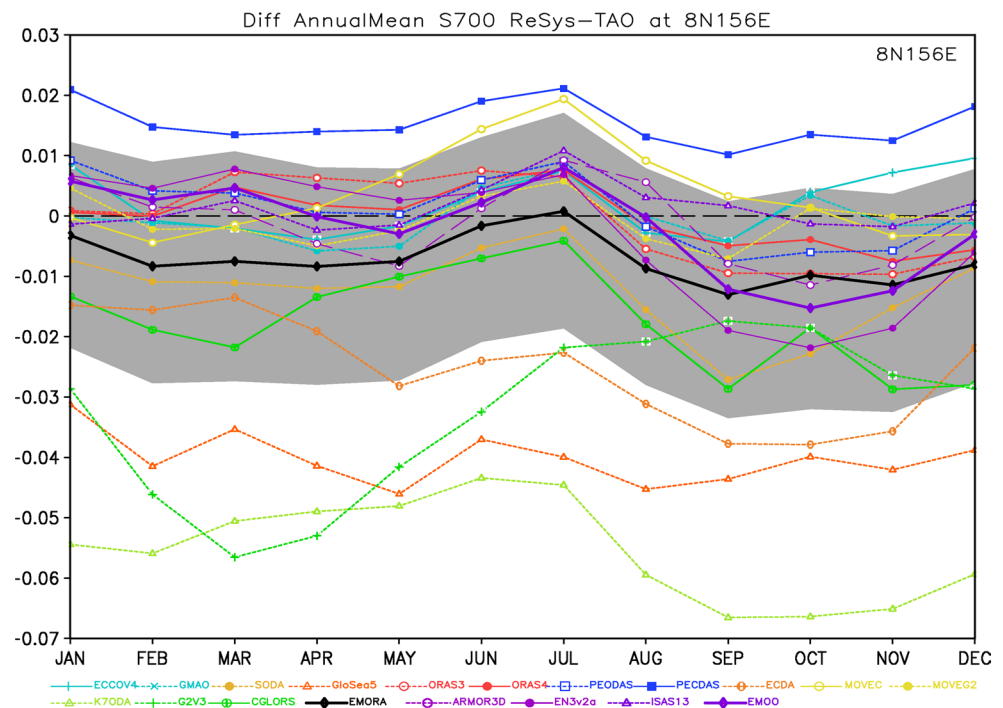
differences in the southern band (averaged over 60°S–30°S; Fig. 2c) is relatively large in the Indian Ocean sector and Pacific Ocean sector, presumably due to sparsity of observations. However, it is relatively lower in the Atlantic sector of the Southern Ocean. K7ODA is seemingly an outlier. This is mainly from the fact that its S700 is calculated under the assumption of constant water volume of the first ocean layer despite a free surface ocean model applied in K7ODA.

The seasonal cycle (i.e., January–December monthly climatology) of S700 for a moored buoy located at 8°N, 156°E (referred as T8N156E) is selected to compare with all products in Table 1 at the same location (by linear interpolation) and same period (1999–2010). The differences in the observed seasonal cycle for each ORA are shown in Fig. 3. This buoy has observations for the longest available period (from February 1999) and covers the most depth layers (from 1.5 to 750 m depth) among all buoy sites of the TAO/TRITON array (available at http://www.pmel.noaa.gov/tao/proj_over/triton.html). Generally, the average UCR_{EMORA}^{SC} (≈0.02 psu; shaded band in Fig. 3; refer to the Eq. (4)) along the seasonal cycle of S700 differences between all ORAs and the T8N156E buoy are significantly smaller than that (≈0.1 psu) in other regions (Fig. 2). The bias of EMOO is comparable to that of EMORA. This is not surprising, given the availability of observations at this specific location. A few individual ORAs show differences comparable with EMOO or EMORA. However, the spread among the ORAs is much larger than the spread among OOAs. This is indicative that errors in ocean models,

surface forcing and data assimilation methods are still an issue for the precise estimation of salinity. For instance, over-estimation of precipitation in the tropical band by most atmospheric reanalyses has been reported by several studies (Janowiak et al. 2010; Kim and Alexander 2013).

4 Temporal variability

4.1 Standard deviation

The first assessment of salinity variability is the standard deviation (*STD*; refer to the Eqs. (7, 8)), which is an important indicator of the amplitude of S700 anomalies[5] (seasonal cycle removed) from all products for the period 1993–2010 (Fig. 4). In the northern band (30°N–60°N average; Fig. 4a), the STD_n^A (refer to the Eq. (7)) of S700 anomalies from most ORAs in the central north Pacific is generally smaller than that in the north-western and north-eastern Pacific, but the UCR_{EMORA}^{STD} (refer to the Eq. (4); shaded band in Fig. 4) is very similar over the whole northern Pacific. In the North Atlantic Ocean, the *STD* of S700 anomalies from all products, as well as the UCR_{EMORA}^{STD}, significantly decreases from west (i.e., the Gulf Stream) to east. The STD_{EMORA}^A [refer to the Eq. (8)] of S700

---

[5] Hereafter, the 'anomalies' in this study are relative to the corresponding January–December monthly climatology (i.e., seasonal cycle).
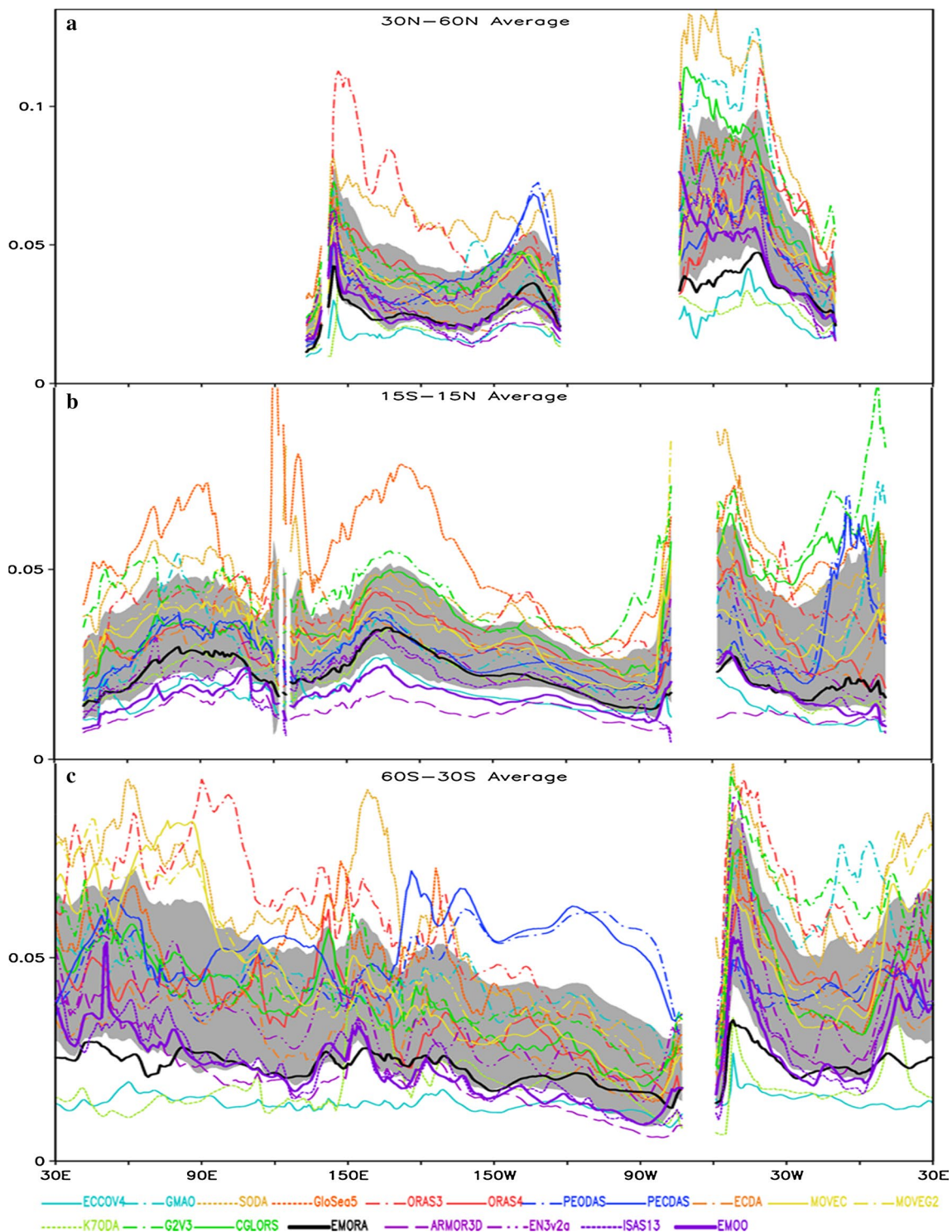
Fig. 4 a Zonal distribution of meridionally-averaged (over 30°N–60°N) temporal standard deviation of S700 anomalies (i.e. STD_n^A) from individual products for the period 1993–2010. The definition of *shaded band* (i.e. UCR_{EMORA}^{STD}) can be referred to the Eq. (4). **b** Same as in **a**, except for except for meridionally-averaged over 15°S–15°N. **c** Same as in **a**, except for meridionally-averaged over 60°S–30°S. The unit of ordinate is psu

anomalies from EMORA agrees well with that from EMOO (i.e., STD_{EMOO}^A; refer to the Eq. (8)) except for the Gulf Stream.

In the tropical oceans (15°S–15°N average; Fig. 4b), the largest UCR_{EMORA}^{STD} occurs in the Atlantic Ocean, especially in the eastern part of the basin. In the Indian Ocean,

the UCR_{EMORA}^{STD} and amplitude of S700 anomalies is largest in the central-eastern Indian Ocean (around 90°E). In the Pacific, both the UCR_{EMORA}^{STD} and the amplitude of the S700 anomalies is largest in the western edge of the West Pacific Warm Pool (WPWP) region (around 165°E), and then, decreases both eastwards and westwards. In contrast, in the Atlantic Ocean the largest STD_n^A from most ORAs, as well as the UCR_{EMORA}^{STD}, is seen in both the east and west (e.g., the Gulf of Guinea). The STD_{EMORA}^A of S700 anomalies from EMORA is consistently larger than the STD_{EMOO}^A from EMOO, especially in the central tropical Indian Ocean, central-western tropical Pacific and western tropical Atlantic Ocean. Most individual ORAs (with the exceptions of ECCOV4 and K7ODA) exhibit higher variability than that of individual OOAs, which highlights the contribution of models and surface forcing to the estimation of salinity variability. The differences in variability of S700 anomalies among the 3 OOAs are not small, even in the tropical Pacific Ocean where there is a relative abundance of observations. ARMOR3D seems to be the outlier, showing very small *STD* of S700 anomalies.

The STD_n^A of S700 anomalies from most ORAs, as well as the UCR_{EMORA}^{STD}, in the Southern Ocean along the ACC region (Fig. 4c) is generally larger than that in the tropical oceans and the northern band. This relatively large UCR_{EMORA}^{STD} is likely caused by the lack of observation that results in the *STD* of S700 anomalies becoming more dependent on the ocean model, assimilation method and atmospheric forcing etc. The STD_{EMORA}^A of S700 anomalies from EMORA is smaller than that of most individual ORAs, and comparable to the STD_{EMOO}^A from EMOO, suggesting a lack of coherence in the variability of individual ORAs. Exceptions are the convergence zone (around 45°W) of the Brazil Current and the South Atlantic Current; the convergence zone (around 15°E) of the Benguela Current and the Agulhas Current. In these dynamically active regions the ocean model is likely to be playing a significant role.

It is worth noting that most ORAs show relatively large *STD* of S700 anomalies than the 3 OOAs over most parts of oceans. Although the amplitude of salinity variability may be overestimated by the model-based ORAs, it is also possible that the 3 OOAs underestimate the variability because in regions of sparse observations they will be closer to climatology. The UCR_{EMORA}^{STD} (up to 0.05 psu) of the STD_n^A of S700 anomalies in Fig. 4 is smaller than that of corresponding AMS700 differences (around 0.1 psu) shown in Fig. 2, except for the tropical Pacific Ocean and the Atlantic sector of the Southern Ocean. Additionally, we note that the STD_{EMORA}^A of EMORA is smaller than that of individual ORA in most cases, except for the tropical Indian-Pacific Ocean. This feature implies that the variability of S700

anomalies from individual ORA is quite diverse, and different from EMORA in most cases. The phase agreement of S700 variability between all individual ORAs and EMOO will be assessed further in the next Sect. 4.2.

There is no specific ORA that is an overall outlier in Figs. 2 and 4. It suggests that no specific ORA is the best or worst one among all 14 ORAs in this study. However, in specific regions there are specific outliers, for example, the K7ODA in the North Atlantic Ocean and the Southern Ocean; the GloSea5 and G2V3 in the tropical Pacific Ocean; the PEODAS and PECDAS in the western tropical Atlantic Ocean.

4.2 Signal-to-noise ratio

The *SPD* of S700 anomalies from each ORA about the corresponding EMORA (refer to SPD_{EMORA}^A in the Eq. (3)) is shown in Fig. 5a. The geographical distribution of the largest SPD_{EMORA}^A of S700 anomalies (≥0.1 psu) is associated with the largest SPD_{EMORA}^{AM} of AMS700 (see Fig. 1c), particularly in the western boundary currents, such as the Kuroshio, Gulf Stream and Brazil Current. Other areas of relatively large SPD_{EMORA}^A of S700 anomalies (≥0.06 psu) can be seen in the sub-tropical eastern Indian Ocean and central Pacific Ocean. As was discussed in Balmaseda et al. (2015), the areas of the relatively large uncertainty in salinity reanalyses tends to occur in regions associated with both strong temperature and salinity fronts. Of course, the effects of the ocean models and assimilation techniques on the uncertainty cannot be discarded.

As mentioned above, the STD_{EMORA}^A of S700 anomalies from EMORA (Fig. 5b), can be considered as a quantitive estimate of the signal. The regions with the largest signal mainly occur in the WPWP region, central Indian Ocean, Gulf of Alaska along the Alaska Current and a narrow band in the Southern Ocean (around 40°S, 20°W–70°E). It is also high in areas of strong variability such as the western boundary currents in Atlantic Ocean. Strong variability occurs in the WPWP due to strong rainfall and current variability.

Following the approach used by Lee et al. (2009) and Zhu et al. (2012); the ratio of the STD_{EMORA}^A (Fig. 5b) to the SPD_{EMORA}^A (Fig. 5a) of S700 anomalies can be considered as the so-called signal to noise ratio (*SNR*) that gives a good quantitative estimate of the reliability of S700 variability among the different ORAs. As shown in Fig. 5c, the regions where the *SNR* is greater than 1 mainly appear in the WPWP region, central tropical Indian Ocean, the Gulf of Alaska and other small regions of the mid-latitude oceans. The relatively large *SNR* over the WPWP, which is also an area of large interannual variability, is likely related to the constraint provided by the salinity

Fig. 5 **a** Distribution of ensemble spread of S700 anomalies (i.e. SPD^A_{EMORA}) from 14 ORAs about the corresponding EMORA for the period 1993–2010. **b** The temporal standard deviation of S700 anomalies from EMORA (i.e. STD^A_{EMORA}) for the period 1993–2010. The unit of *colour bar* in **a**, **b** is psu. **c** The distribution of the estimated signal-to-noise ratio (*SNR*) of S700 anomalies from 14 ORAs for the period 1993–2010
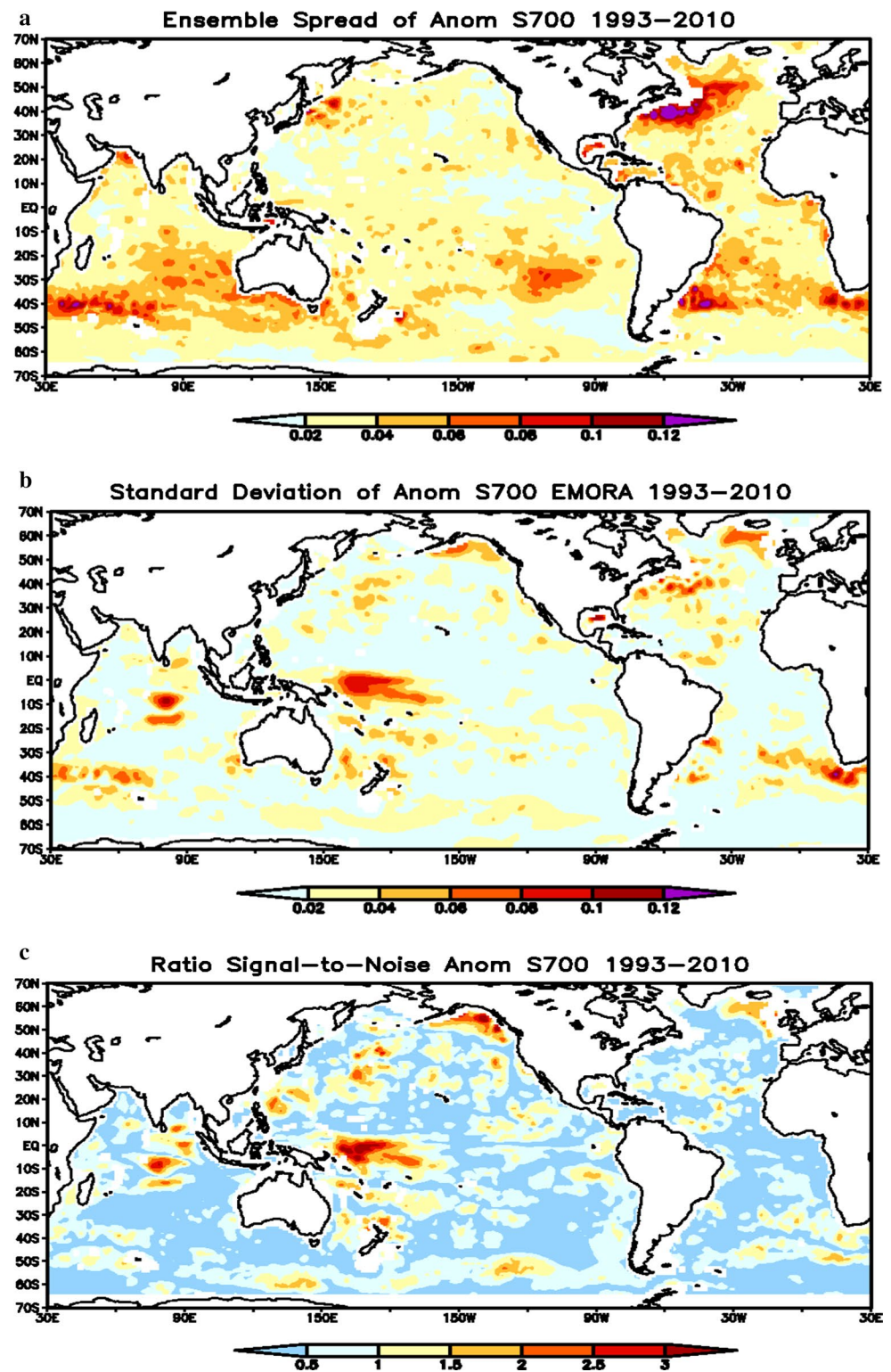
observations from the TAO/TRITON moorings. Overall, the *SNR* is less than 1 over most parts of oceans, indicating that there is relatively large SPD^A_{EMORA}, and therefore, disagreement in the estimates of S700 anomalies among different ORAs.

4.3 Correlation

Figure 6a illustrates how well the S700 variability in the two ensemble means agree with each other. Correlations are relatively high ($\geq$0.75) in the central and western equatorial
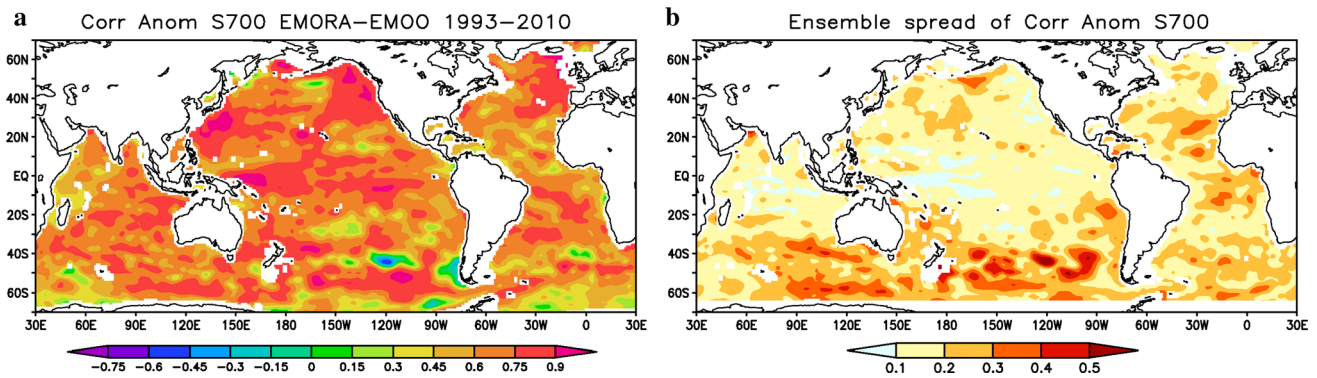
Fig. 6 **a** Temporal correlation coefficients of S700 anomalies between EMORA and EMOO for the period 1993–2010. **b** Ensemble spread (i.e. SPD^{COR}_{EMORA}) of correlation coefficients of S700 anomalies between individual ORAs and EMOO about their mean correlation coefficients

Pacific, western sub-tropical Pacific along the Kuroshio and north-eastern mid-latitude Pacific. They are also high in the eastern equatorial Indian Ocean, and throughout parts of the sub-tropical and mid-latitude oceans. Correlations are relatively low (≤ 0.5) around the northern edge of the ACC, western Indian Ocean and parts of the sub-tropical Atlantic, particularly downstream of the Mediterranean outflow.

The S700 variability of each ORA can be correlated with that of EMOO. And then, the SPD^{COR}_{EMORA} of the correlations from 14 ORAs about their corresponding ensemble average of all 14 correlations (refer to the Eq. (2) for details) provide an indication of the disagreement in the estimate of variability between the different systems (Fig. 6b). There is some correspondence between areas with large SPD^{COR}_{EMORA} and low correlation in Fig. 6a, such as the northern edge of the ACC in the Pacific sector and the northern part of the tropical Atlantic. Equally, the high correlation in the Tropical Pacific, Eastern Indian Ocean, North East Pacific and North East Atlantic, where the spread is low, is indicative of consistency between the different estimates. The Southern Ocean is an exception, showing relatively large values of the correlation and the SPD^{COR}_{EMORA}.

The WPWP region and central tropical Indian Ocean, the regions with the smallest SPD^{COR}_{EMORA} (best agreement among all ORAs, Fig. 6b), also have the highest *SNR* values (Fig. 5c). It is worth noting that these regions are also the places where the largest precipitation variability occurs (Storto et al. 2015).

Figure 7 shows the zonal distributions of the correlation of S700 anomalies between each ORA and EMOO for the period 1993–2010. EMORA, unsurprisingly, obtains the highest correlation among all ORAs over most parts of oceans due to averaging out the impacts of different ocean models, forcing fields and assimilation techniques etc. Generally, the areas of relatively high correlation, associated with relatively small UCR^{COR}_{EMORA} (refer to the Eq. (4)), are in the eastern tropical Indian Ocean, central-western tropical Pacific and north-east Pacific. In contrast, the areas of

relatively low correlations, associated with relatively large UCR^{COR}_{EMORA}, are in the Southern Ocean and the tropical and north-west Atlantic Ocean.

4.4 Local T–S correlation

The close relationship between seawater temperature and salinity (T–S) is too complicated to be precisely described and measured in one simple way. However, in this study, we utilize the correlation between the local S700 anomaly and the corresponding depth-averaged temperature (over upper 0–700 m ocean layer, referred as T700) anomaly to investigate how the co-variability between T700 and S700 anomalies represented by the ORAs compares with that of EMOO. Figure 8a, b show the temporal correlation between the T700 anomaly and S700 anomaly from EMORA (Fig. 8a) and EMOO (Fig. 8b) for the period 1993–2010. The distribution of T700–S700 correlations from EMORA is quite similar to those of EMOO, showing coherent large scale patterns. For instance, relatively high positive correlation in most parts of Atlantic Ocean, equatorial Pacific, north-eastern and southern sub-tropical Pacific, southern sub-tropical Indian Ocean; whereas, negative correlations mainly occur in the eastern equatorial Indian Ocean, the north-eastern boundary of the Pacific (i.e., off the east coast of Mexico and the Gulf of Alaska), and in particular the Southern Ocean. However, EMORA (Fig. 8a) produces more extreme positive and negative correlation than EMOO (Fig. 8b). Yet, the region of negative correlation for EMORA is smaller than that of EMOO, in particular the narrower negative correlation belt in the Southern Ocean in Fig. 8b. It seems that most ORAs exhibit a stronger relationship between the local salinity content and heat content compared to EMOO, in particular in the north-west Indian Ocean, the equatorial Atlantic Ocean, and the northern edge of the ACC in the Indian-Pacific Ocean sector. In this area, where there are few temperature and salinity observations,

Fig. 7 a Zonal distribution of meridionally-averaged (over 30°N–60°N) correlation coefficients of S700 anomalies between individual ORAs and EMOO for the period 1993–2010. The definition of

shaded band (i.e. UCR_{EMORA}^{COR}) can be referred to the Eq. (4). **b** Same as in **a**, except for meridionally-averaged over 15°S–15°N. **c** Same as in **a**, except for meridionally-averaged over 60°S–30°S

the associated relationship between local salinity and temperature in the ORAs may come from the ocean-model information, which is absent in the OOAs.

There is no unique explanation for the large scale patterns of correlation between T700 and S700. It is possible that changes associated with local vertical displacement of
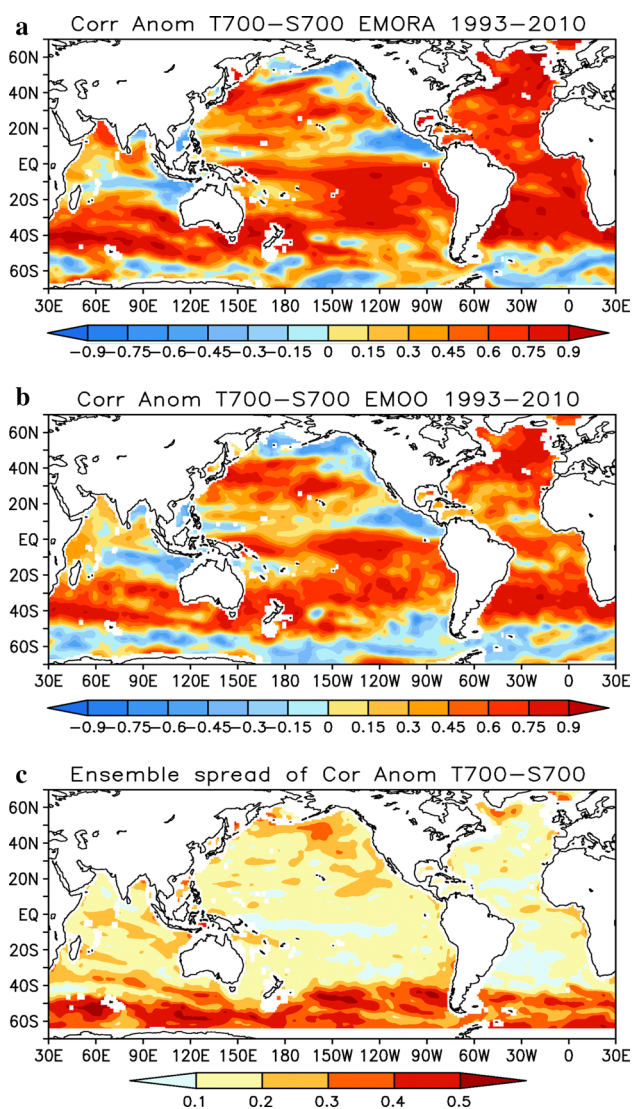
Fig. 8 **a** Temporal correlation coefficients between S700 anomalies and T700 anomalies from EMORA for the period 1993–2010. **b** Same as in **a**, except for EMOO. **c** Ensemble spread (i.e. SPD_{EMORA}^{COR}) of T700–S700 anomalies correlation coefficients from individual ORAs about their mean correlation coefficients

the water column related with, say, variations in Ekman pumping, would result in positive/negative correlation of T700–S700 wherever the temperature and salinity vertical stratification (above and below 700 m) has the same/opposite sign. But changes associated with horizontal displacement of water masses, or changes in the water mass properties cannot be discarded either.

Figure 8c shows the SPD_{EMORA}^{COR} (refer to the Eq. (2) for details) of the T700–S700 correlation from all ORAs about the corresponding ensemble average correlation (refer to $\overline{X_{EMORA}}$ in the Eq. (1)) for the period 1993–2010. The largest SPD_{EMORA}^{COR} of the T700–S700 correlation among the ORAs occurs in the Southern Ocean. This disagreement can

be attributed to the lack of observations in this region, and to the different T700–S700 correlation among ocean models.

The zonal distributions of T700–S700 correlation from each ORA are shown in Fig. 9. The correlations from most ORAs agree quite well with that of the OOAs in some parts of ocean, for instance, in the mid-latitude North Pacific and the eastern tropical Pacific. In some other parts of oceans, however, the correlation of most ORAs is higher than that of OOAs, such as in the central-western tropical Pacific, central tropical Indian Ocean, the Southern Ocean in both Indian Ocean sector and east Pacific sector, and in particular in the tropical Atlantic Ocean where the correlation of OOAs is around 0.4 but the correlations of most ORAs are generally more than 0.6 (Fig. 9b). In the tropical Indonesian Sea/eastern Indian Ocean area (90°E–130°E), most ORAs show negative local T700–S700 correlations (up to −0.6; Fig. 9b). We suspect this may be attributed to the Indonesian Throughflow (ITF) transporting relatively warmer and fresher sea water from the Pacific Ocean into the Indian Ocean (Vranes et al. 2002; Sprintall et al. 2009).

4.5 Impacts of Argo

Figure 10 shows the depth/time evolution (1993–2010) of the centred pattern correlation coefficients[6] (i.e., *CPCOR*; refer to the Eq. (9); Santer et al. 1993; von Storch and Navarra 1999) of salinity anomalies between EMORA and EMOO, averaged over 0–360°E; 30°N–60°N (Fig. 10a); 15°S–15°N (Fig. 10b); 60°S–30°S (Fig. 10c), respectively. The vertical distribution of *CPCOR* in both the mid-latitude northern oceans (Fig. 10a) and the tropical oceans (Fig. 10b) generally decrease downwards from 100 to 1500 m depth. Relatively high correlation (≥ 0.5) is obtained over the upper 300–400 m depth before 2001, and then, increases up to more than 0.9 and extended to 500–600 m depth after 2002. This increase corresponds quite well with the beginning of the Argo project. The relatively higher *CPCOR* within the upper 500 m ocean layer in both mid-latitude and tropical oceans after 2002 indicates higher consistency in the estimated pattern of salinity anomalies by both EMORA and EMOO due to Argo. The *CPCOR* decreases downwards with the depth increasing, and is likely attributed to a lack of coherence between the anomaly patterns from EMORA and EMOO.

In contrast, the vertical distribution of *CPCOR* in the Southern Ocean band (Fig. 10c), increases downward from the surface to 1500 m depth before 2002. The reason for this feature needs to be investigated further. This may be related to the existence of slowly varying spatial salinity

---
[6] A 7-month running mean has been applied on the computed correlation coefficients to remove the intra-seasonal variability.
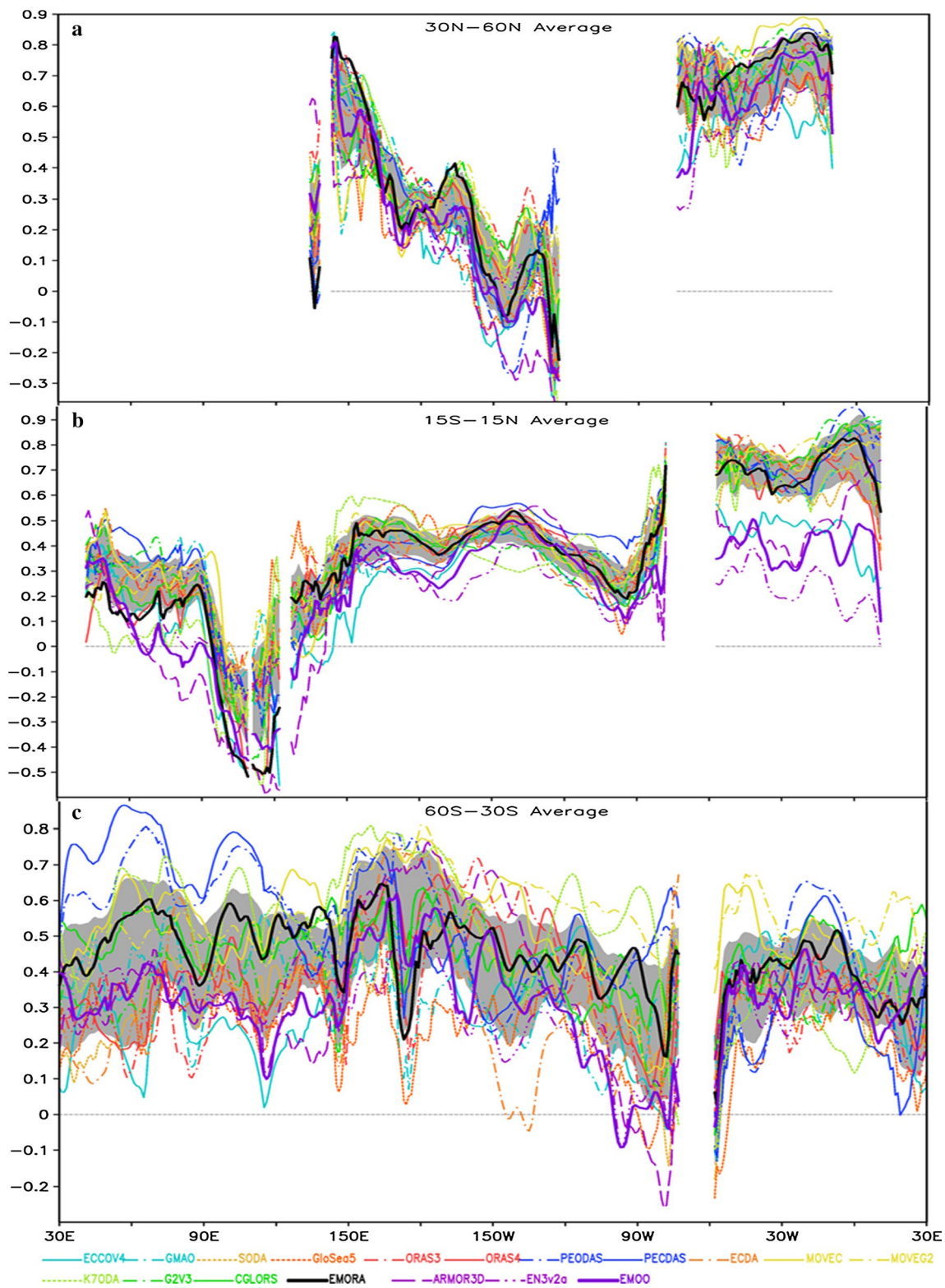
Fig. 9 Same as in Fig. 7, except for correlation coefficients between the T700–S700 anomalies

patterns at these latitudes, which can be sample even with a limited set of observations. A large value of the correlation is not synonymous of adequate sampling though. The

influence of a few deep observations may also persist for longer in the slowly varying deep ocean. Hence, the relatively higher correlation in the deep Southern Ocean prior

Fig. 10 **a** Centred pattern correlation coefficients (i.e. *CPCOR*; calculated over the band area 0–360°E; 30°N–60°N) of salt anomalies between EMORA and EMOO as a function of depth (0–1500 m) and time (1993–2010. Prior to plotting a 7-month running mean was applied on the computed correlation coefficients to remove the intra-seasonal variability. The ordinate has units meter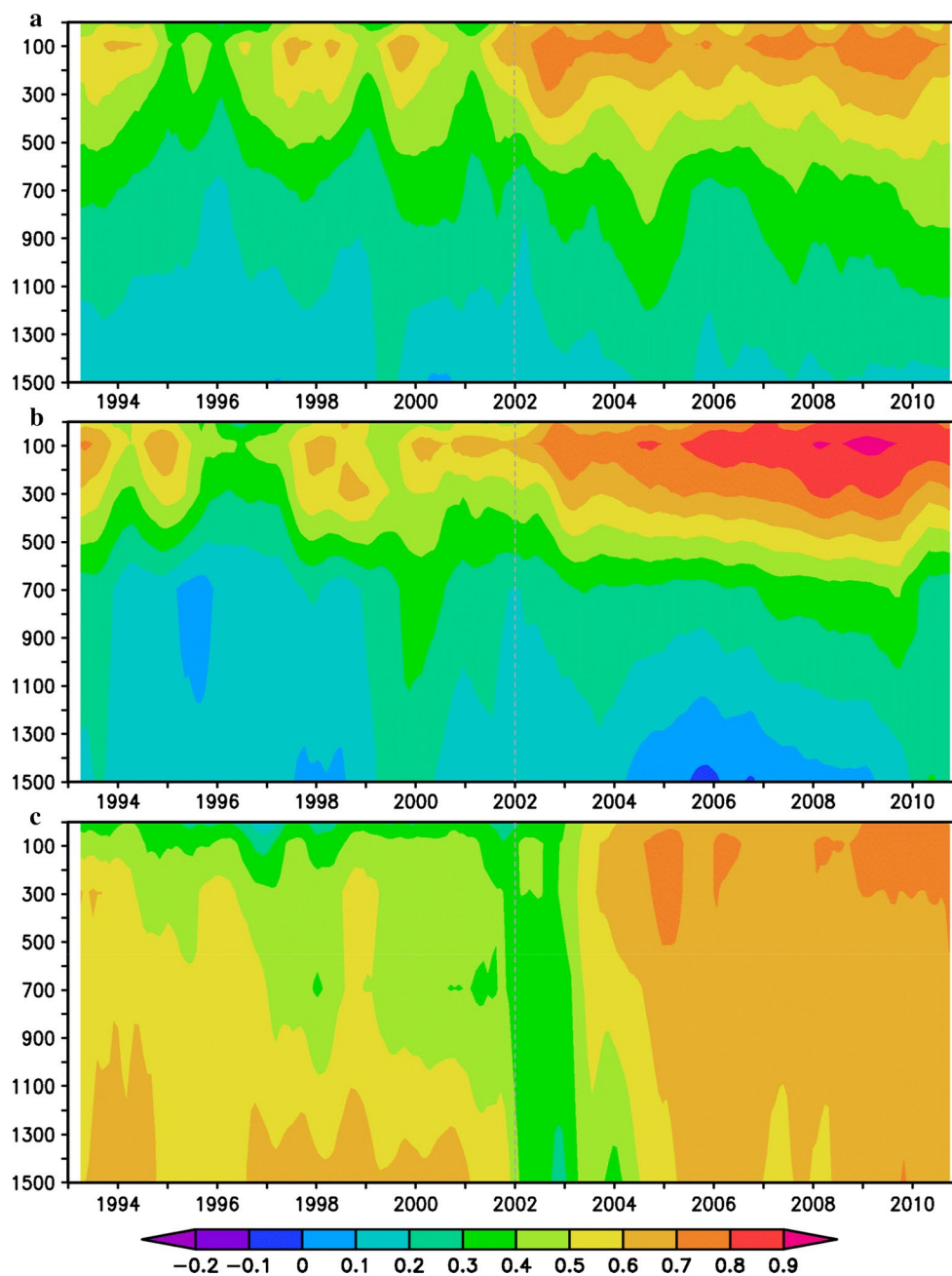 (m). **b** Same as in **a**, except for the band area 0–360°E; 15°S–15°N. **c** Same as in **a**, except for the band area 0–360°E; 60°S–30°S

to Argo may be also an artefact of using climatology in all the estimates, either as a prior in the OOAs, or as a nudging term in the ORAs. There is a period of lower spatial correlations during 2003, probably associated with the diversity of ways in which different systems adjust to the spin-up of Argo (including different quality control decisions).Since 2003, the correlation in the Southern Ocean also increases over the 0–1000 m depth, in particular over 0–400 m depth after 2009, as Argo floats were deployed.

Generally, after Argo the *CPCOR* over the upper 0–500 m of the ocean in both northern and southern mid-latitude oceans are significantly smaller than that in the

tropical oceans. This indicates that there is still room for the salinity reanalyses in both northern and southern mid-latitude oceans to be further improved and highlights the need for more Argo floats in this region.

5 Trend

A phenomenon, which has been noticed by previous studies (Levitus et al. 2009; Xue et al. 2012; Balmaseda et al. 2015; Palmer et al. 2015) and announced by the IPCC (2013) and operational or research centres

Fig. 11 a Evolution of global averaged (over 0–360°E; 60°S–60°N) and depth-averaged (within 0–300 m ocean layer) salinity anomalies from all products for the period 1993–2010. The definition of *shaded band* (i.e. UCR^A_{EMORA}) can be referred to the Eq. (5). The unit of ordinate is psu. **b, c** Same as in **a**, except for depth-averaged salinity anomalies within 300–700 m layer and 700–1500 m layer, respectively. Prior to plotting a 7-month running mean was applied to remove the intra-seasonal variability
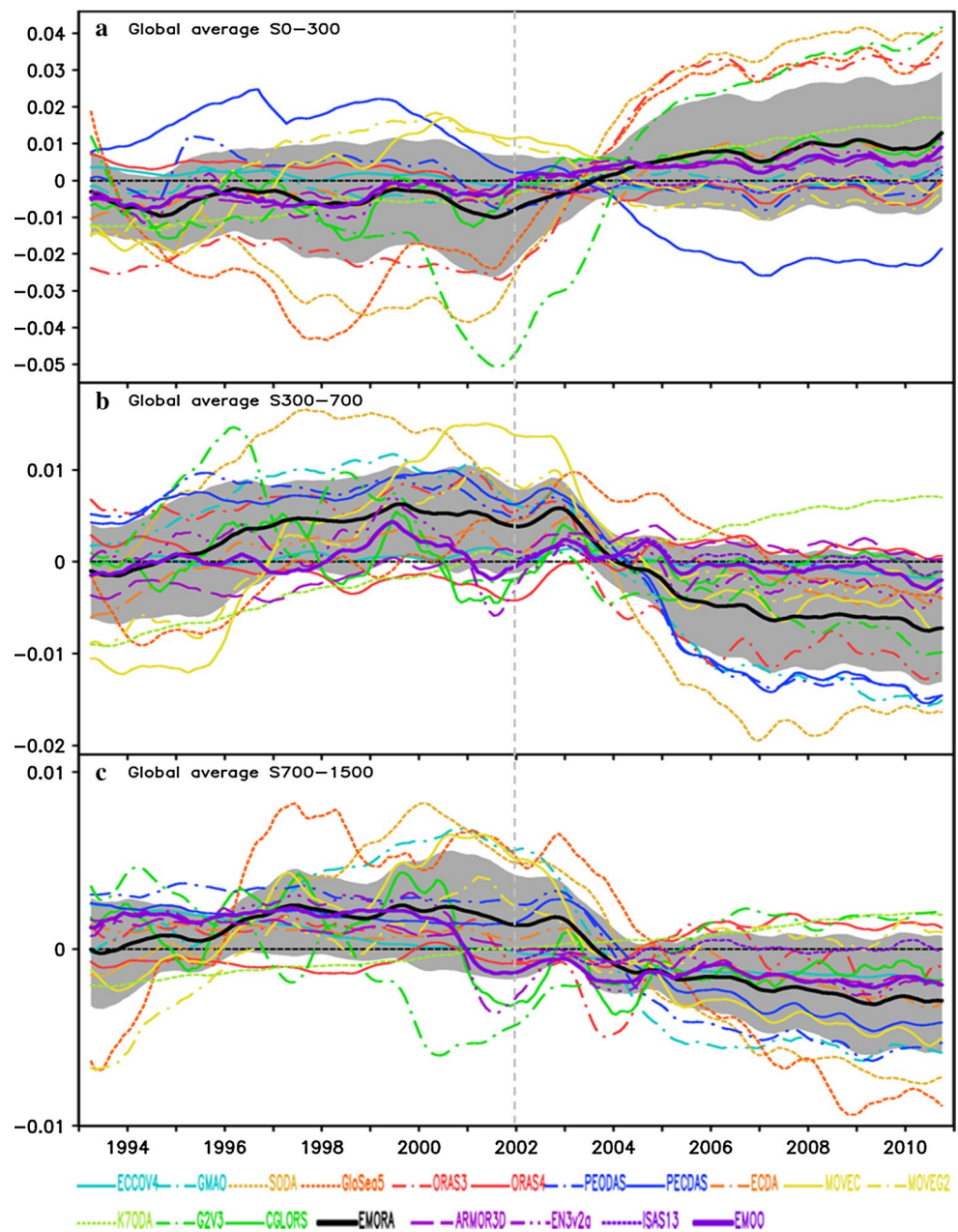
(http://www.epa.gov/climatechange/science/indicators/oceans/ocean-heat.html), is that the global averaged ocean heat content anomalies from either ORAs or OOAs have a growing trend from the 1990s till now. A similar growing trend has also been found in the steric sea level change (Levitus et al. 2012; also http://www.nodc.noaa.gov/OC5/3M_HEAT_CONTENT). This warming trend of ocean heat content anomalies has been considered as strong evidence for global warming in recent decades (IPCC 2013). Therefore, an interesting question is if the corresponding global averaged salinity anomalies retain a similar growing trend since the 1990s? If so, since the total salinity is approximately conserved in the global ocean, are the salinity anomalies

that show a growing trend within a certain ocean layer compensated with a decreasing trend at other depths?

Figure 11a–c shows the temporal evolution of global averaged (0–360°E; 60°S–60°N) salinity anomalies (relative to climatology for the period 1993–2010), depth-averaged within 0–300 m (i.e., S300; Fig. 11a), 300–700 m (i.e., S3-700; Fig. 11b) and 700–1500 m (i.e., S7-1500; Fig. 11c) ocean layers, from all products for the period 1993–2010. It is worth noting that the depth-average in this study is calculated within 3 continuous vertical layers (i.e., 0–300; 300–700 and 700–1500 m) rather than the top to bottom vertical average (e.g., 0–300, 0–700 and 0–1500 m) approach used by Balmaseda et al. (2015). Therefore, we can show the

different features of the trend in salinity anomalies within different vertical layers. In addition, the reference period for the climatology in this study (1993–2010) is different to the 1993–2007 period used by Balmaseda et al. (2015).

In the 0–300 m upper ocean (Fig. 11a), the temporal evolution of global averaged S300 anomalies from all 3 OOAs, EMOO and EMORA show a growing trend similar to the corresponding global averaged temperature anomalies (not shown). However, the temporal evolutions of global averaged S300 anomalies among different ORAs are quite divergent and with a relatively large UCR^A_{EMORA} (refer to the Eq. (5)). For instance, SODA, GloSea5, ORAS3 and G2V3 show rapidly growing trends after the beginning of Argo (2001), in contrast, PECDAS shows a decreasing trend since the end of the 1990s and most other ORAs show weak decreasing and increasing trends. In contrast, it can be seen from Fig. 11b that the temporal evolution of the S3-700 anomalies from most ORAs shows a trend turning from generally increasing to decreasing after 2003. For all OOAs and a few ORAs, such as the ORAS4, CGLORS, there is no clear trend before 2003 followed by a very weak decreasing trend after 2003. This feature is quite different from that of the corresponding global average temperature anomalies (not shown). Within the 700–1500 m depth layer, for the S7-1500 anomalies (Fig. 11c), most ORAs and OOAs, except for the G2V3, ORAS4 and K7ODA, show a decreasing trend in the reference period, in particular after the beginning of Argo.

Generally, the global averaged S300 anomalies from most ORAs and OOAs show a similar growing trend in the reference period as that shown in corresponding global averaged temperature anomalies, even though there is an increasing discrepancy of S300 anomalies among different ORAs, in particular after the beginning of Argo. As the ocean depth increases, the global averaged salinity anomalies from most ORAs and OOAs show a decreasing trend, in particular after Argo. This feature can probably be explained by the approximate conservation of salt in the global ocean. Interestingly, it can be seen from Fig. 11 that most ORAs show a rapid change in both salinity and temperature anomalies (not shown) after the beginning of Argo (i.e., 2002 or 2003). We note it is more likely caused by the changes before and after Argo because of the shortage of reliable observations of both salinity and temperature (in particular in the subsurface ocean) prior to the Argo project.

6 Conclusions

In this paper, the reanalysed S700 of 14 ORAs from different institutions is assessed to address the major agreement/disagreement among different ORAs. All ORAs assimilate both temperature and salinity observations using a variety of ocean models and assimilation methods. In addition, three OOAs are also used in this paper as independent data and reference for the assessment. The ensemble spread about the multi-system ensemble mean is utilized to demonstrate the agreement/disagreement and measure the uncertainty range among different ORAs.

Generally, the largest agreement (or smallest uncertainty range) of reanalysed S700 properties, such as mean state, standard deviation and correlation, among different ORAs occurred in the tropical Pacific. The largest disagreement (or uncertainty range) was found in the Southern Ocean along the ACC, and along the western boundary currents, such as the Kuroshio, Gulf Stream and Brazil Current. The main cause for the disagreement in the Southern Ocean can be attributed to both the shortage of ocean and atmospheric observations. Assimilation in the regions along the western boundary currents, in particular the Gulf Stream, can be more difficult as noted by Balmaseda et al. (2015) because the relatively stronger ocean fronts in these regions are not well simulated by the ocean models.

It is shown that the variability of S700 anomalies (i.e., standard deviation) from most of the ORAs is usually stronger over most parts of oceans compared with that from the OOAs. Moreover, the standard deviation of EMORA is smaller than that of most individual ORAs over most parts of oceans, except for the tropical Indian-Pacific Ocean. This is because there is relatively large phase dispersion among different ORAs in these regions. Consequently, EMORA obtains the highest correlation of S700 anomalies with the corresponding EMOO when compared with that of each ORA. A *SNR* value larger than one is mainly restricted to the WPWP region (probably because of the TAO/TRITON salinity observations), the central tropical Indian Ocean and a few parts of the north Pacific and is associated with the regions with the smallest disagreement of S700 anomalies correlations among different ORAs.

Correlations between T700 and S700 anomalies show coherent high values and consistent spatial patterns in both ORAs and OOAs products. The reason for this coherent large scale behaviour needs to be explored further. It may be caused by the temporal variations in availability of observations, which would affect ORAs and OOAs in similar manners. But it may be indicative of real dynamical signals associated to the large scale ocean circulation. Having good salinity estimations can thus help us with the understanding and attribution of ocean variability.

The impact of Argo floats on the ocean reanalyses has been shown by some previous studies (Balmaseda et al. 2007). In this study, our results demonstrated that the tropical oceans/Southern Ocean have the largest/smallest improvement of salinity reanalyses during the Argo period. Interestingly, the relatively large improvements in the salinity reanalyses due to Argo are mainly confined within the

upper 500 m. It's probably because the models have better physics in the upper ocean and therefore fit the Argo data in the upper ocean better. We note that the reason for this phenomenon need to be further investigated in the future.

Although the assimilated global heat content anomalies within upper 700 m from most ORAs and OOAs show an increasing trend during the reference period 1993–2010 (refer to Palmer et al. 2015), the global averaged salinity anomalies from most ORAs and OOAs only show an increasing trend within the top 0–300 m layer, in particular in the Argo period. In contrast, in the other two layers beneath 300 m (i.e., 300–700; 700–1500 m), the global averaged salinity anomalies from most ORAs and OOAs switch their trends from a slightly increasing trend prior to Argo to a decreasing trend after Argo. We note that there is a rapid change in the trend in global averaged salinity anomalies around 2002 likely due to Argo.

While there is some agreement regarding the spatial patterns of interannual variability of salinity and its relation with temperature, large uncertainty remains regarding global averaged salinity anomaly trends that will affect the estimation of global steric height (Zuo et al. 2015). Since conservation of salt content is considered to be a good approximation, for diagnostic and attributions studies of global sea level it may be more pertinent to ignore the halo-steric component, rather than using unreliable halo-steric trends from ORAs. However, the ORA estimation of the thermo-steric component appears to be more robust (Storto et al. 2015).

Finally, despite the progresses in salinity reanalyses made by most state-of-the-art ORAs, we note that the current performance of salinity reanalyses from most ORAs is still a long way from being considered a satisfactory and reliable estimation. As mentioned above, the relatively large disagreement/agreement in reanalysed salinity among the different ORAs offers a useful guidance to potential users and scientists. These results highlight ocean regions where the salinity reanalyses may be more reliable (e.g., the tropical Pacific Ocean) and which regions the salinity reanalyses need to be improved (e.g., the Southern Ocean and regions along the western boundary currents). Sustaining and enhancing oceanic measurements of salinity such as those derived from Argo and satellites (e.g., European Space Agency's Soil Moisture and Ocean Salinity and NASA's Aquarius missions) and improving evaporation and precipitation products (e.g., from atmospheric reanalysis) are important to improving the representation of salinity by ORAs in the future. It is also worth noting that the impacts of the ocean models and assimilation techniques on the improvement of salinity reanalyses are also important.

Appendix

Multi-system ensemble mean

In this study, the X_n^A represents the anomaly (seasonal cycle removed) of corresponding total variable X_n for individual n ORA. Thus, the multi-system ensemble mean (i.e., EMORA) of X_n or X_n^A from the 14 ORAs can be given by:

$$\overline{X_{EMORA}} = \frac{1}{nsys}\sum_{n=1}^{nsys}X_n \quad \text{or} \quad \overline{X_{EMORA}^A} = \frac{1}{nsys}\sum_{n=1}^{nsys}X_n^A \quad (1)$$

The $nsys$ represents the total number of all ORAs for calculating EMORA ($nsys = 14$). The corresponding $\overline{X_{EMOO}}$ or X_{EMOO}^A can be similarly calculated by the Eq. (1) except for the X_n or X_n^A of individual n OOA and $nsys = 3$.

Ensemble spread (SPD)

The ensemble spread of different variables X from 14 ORAs about their corresponding EMORA shown in Figs. 1c, 6b and 8c is given by:

$$SPD_{EMORA}^X(i,j) = \sqrt{\frac{1}{nsys}\sum_{n=1}^{nsys}\left(X_n(i,j) - \overline{X_{EMORA}}(i,j)\right)^2} \quad (2)$$

Here, the X represents the annual mean (AM) of S700 in Fig. 1c (i.e., SPD_{EMORA}^{AM}), the correlation of S700 anomalies in Fig. 6b and the correlation of T700–S700 anomalies in Fig. 8c (i.e., SPD_{EMORA}^{COR}), respectively. The i/j represents the longitude/latitude, respectively.

Similarly, the $SPD_{EMORA}^A(i,j)$, that is shown in Fig. 5a, can be calculated as:

$$SPD_{EMORA}^A(i,j)$$
$$= \sqrt{\frac{1}{mons}\sum_{t=1}^{mons}\frac{1}{nsys}\sum_{n=1}^{nsys}\left(X_n^A(i,j,t) - \overline{X_{EMORA}^A}(i,j,t)\right)^2}$$
$$(3)$$

Here, the $X_n^A(i,j,t)$ denotes the S700 anomalies for individual n ORA. The $mons$ is the total number of months for the variable X (i.e., $mons = 216$ for the period 1993–2010).

Uncertainty range (UCR)

The uncertainty range (i.e., the shaded band shown in Fig. 2) of the meridionally-averaged AMS700 (i.e., X) from 14 ORAs about their corresponding EMORA (i.e., $\overline{X_{EMORA}}$) is defined as:

$$UCR_{EMORA}^{AM}(i) = \overline{X_{EMORA}}(i) \pm SPD_{EMORA}^{AM}(i) \tag{4}$$

Here, the $SPD_{EMORA}^{AM}(i)$ can be calculated by the Eq. (2) but without the dimension j. The UCR shown in Figs. 4, 7 and 9 can be similarly calculated by the Eq. (4) except that the variable X should be replaced by standard deviation for Fig. 4, the correlation coefficients for Figs. 7 and 9, respectively. In addition, the UCR shown in Fig. 3, where the X represents the seasonal cycle of S700, can be also calculated by the Eq. (4) except for replacing the dimension i by the dimension t.

The $UCR_{EMORA}^{A}(z,t)$ shown in Fig. 11 is given by:

$$UCR_{EMORA}^{A}(z,t) = \overline{X_{EMORA}^{A}}(z,t) \pm SPD_{EMORA}^{A}(z,t) \tag{5}$$

Here, the $\overline{X_{EMORA}^{A}}(z,t)$ denotes the global averaged salinity anomaly in different ocean layers z for EMORA. And, the $SPD_{EMORA}^{A}(z,t)$ is calculated as:

$$SPD_{EMORA}^{A}(z,t) = \sqrt{\frac{1}{nsys}\sum_{n=1}^{nsys}\left(X_n^A(z,t) - \overline{X_{EMORA}^{A}}(z,t)\right)^2} \tag{6}$$

Here, the $X_n^A(z,t)$ denotes the global averaged salinity anomaly in different ocean layers z for the individual n ORA.

Standard deviation (STD)

The STD of the meridionally-averaged S700 anomalies (i.e., $X_n^A(i,t)$) for individual n ORA (i.e., $STD_n^A(i)$) and the corresponding EMORA (i.e., $STD_{EMORA}^A(i)$), which is shown in Fig. 4, is respectively given by:

$$STD_n^A(i) = \sqrt{\frac{1}{mons}\sum_{t=1}^{mons}\left(X_n^A(i,t)\right)^2} \tag{7}$$

and

$$STD_{EMORA}^A(i) = \sqrt{\frac{1}{mons}\sum_{t=1}^{mons}\left(\overline{X_{EMORA}^A}(i,t)\right)^2} \tag{8}$$

The corresponding $STD_{EMOO}^A(i)$ in Fig. 4 can be similarly calculated by the Eq. (8) except for replacing the $X_{EMORA}^A(i,t)$ by the $X_{EMOO}^A(i,t)$. Additionally, the STD of S700 anomaly for EMORA (i.e., $STD_{EMORA}^A(i,j)$), which is shown in Fig. 5b, can be also calculated by Eq. (8) except for adding the dimension j.

Centred pattern correlation (CPCOR)

The centred pattern correlation (i.e., $CPCOR(z\ t)$) of salinity anomalies (seasonal cycle removed) between EMORA (i.e., $\overline{X_{EMORA}^A}(i,j,z,t)$) and EMOO (i.e., $\overline{X_{EMOO}^A}(i,j,z,t)$) as a function of depth (0–1500 m) and time (1993–2010), which is shown in Fig. 10, is defined as:

$$CPCOR(z,t) = \left[\frac{1}{m \times n}\sum_{j=1}^{n}\sum_{i=1}^{m}\left(\left(\overline{X_{EMORA}^A}(i,j,z,t) - M_{EMORA}\right)\right.\right.$$
$$\left.\left.\times\left(\overline{X_{EMOO}^A}(i,j,z,t) - M_{EMOO}\right)\right)\right]\Big/(S_{EMORA}S_{EMOO}) \tag{9}$$

Here, the m/n denotes total longitude/latitude grids of the calculated ocean band. The M_{EMORA}/M_{EMOO} denotes the total mean of the $\overline{X_{EMORA}^A}(i,j,z,t)/X_{EMOO}^A(i,j,z,t)$ over the calculated ocean band, respectively. Thus, the M_{EMORA} can be given by:

$$M_{EMORA} = \frac{1}{m \times n}\sum_{j=1}^{n}\sum_{i=1}^{m}\overline{X_{EMORA}^A}(i,j,z,t) \tag{10}$$

The M_{EMOO} can be similarly calculated by the Eq. (10) except for replacing the $\overline{X_{EMORA}^A}$ by the $\overline{X_{EMOO}^A}$. The S_{EMORA}/S_{EMOO} in Eq. (10) denotes the spatial standard deviations of the X_{EMORA}^A/X_{EMOO}^A, respectively. The S_{EMORA} can be obtained by:

$$S_{EMORA}(z,t) = \sqrt{\frac{1}{m \times n}\sum_{j=1}^{n}\sum_{i=1}^{m}\left(\overline{X_{EMORA}^A}(i,j,z,t) - M_{EMORA}\right)^2} \tag{11}$$

The corresponding S_{EMOO} can be also obtained by the Eq. (11) except for replacing the $\overline{X_{EMORA}^A}$ by the $\overline{X_{EMOO}^A}$.

References

Ballabrera-Poy J, Murtugudde R, Busalacchi AJ (2002) On the potential impact of sea surface salinity observations on ENSO predictions. J Geophys Res 107(C12):8007. doi:10.1029/2001JC000834

Balmaseda MA, Anderson D, Vidard A (2007) Impact of Argo on analyses of the global ocean. Geophys Res Lett 34:L16605. doi:10.1029/2007GL030452

Balmaseda MA, Vidard A, Anderson D (2008) The ECMWF ORA-S3 ocean analysis system. Mon Weather Rev 136:3018–3034

Balmaseda MA, Alves OJ, Arribas A, Awaji T, Behringer DW, Ferry N, Fujii Y, Lee T, Rienecker M, Rosati T, Stammer D (2009) Ocean initialization for seasonal forecasts. Oceanography 22:154–159

Balmaseda MA, Mogensen K, Weaver A (2013) Evaluation of the ECMWF ocean reanalysis ORAS4. Q J R Meteor Soc 139:1132–1161

Balmaseda MA et al (2015) The ocean reanalyses intercomparison project (ORA-IP). J operational oceanography 7:81–99

Behringer DW, Xue Y (2004) Evaluation of the global ocean data assimilation system at NCEP: The Pacific Ocean. In: Eighth symposium on integrated observing and assimilation systems for atmosphere,

oceans, and land surface, AMS 84th annual meeting, Washington State Convention and Trade Center, Seattle, Washington

Belkin IM (2004) Propagation of the "great salinity anomaly" of the 1990s around the northern North Atlantic. Geophys Res Lett 31:L08306. doi:10.1029/2003GL019334

Belkin IM, Levitus S, Antonov J, Malmberg SA (1998) "Great salinity anomalies" in the North Atlantic. Prog Oceanogr 41:1–68

Boyer TP, Levitus S, Antonov I, Locarnini RA, Garcia HE (2005) Linear trends in salinity for the World Ocean, 1955–1998. Geophys Res Lett 32:L01604. doi:10.1029/2004GL021791

Carton JA, Giese BS (2008) A reanalysis of ocean climate using simple ocean data assimilation (SODA). Mon Weather Rev 136:2999–3017

Chang Y-S, Zhang S, Rosati A, Delworth T, Stern WF (2012) An assessment of oceanic variability for 1960–2010 from the GFDL ensemble coupled data assimilation. Clim Dyn. doi:10.1007/s00382-012-1412-2

Cooper NS (1988) The effect of salinity on tropical ocean model. J Phys Oceanogr 18:697–707

Cronin MF, McPhaden MJ (1998) Upper ocean salinity balance in the western equatorial Pacific. J Geophys Res 103:27567–27588

Curry R, Dickson B, Yashayaev I (2003) A change in the freshwater balance of the Atlantic Ocean over the past four decades. Nature 426:826–829

Dickson RR, Meincke J, Malmberg SA, Lee AJ (1988) The "great salinity anomaly" in the northern North Atlantic, 1968–1982. Prog Oceanogr 20:103–151

Durack PJ, Wijffels SE (2010) Fifty-year trends in global ocean salinities and their relationship to broad-scale warming. J Clim 23:4342–4362

Durack PJ, Wijffels SE, Matear RJ (2012) Ocean salinities reveal strong global water cycle intensification during 1950 to 2000. Science 336:455–458

Fedorov AV, Pacanowski RC, Philander SG, Boccaletti G (2004) The effect of salinity on the wind-driven circulation and the thermal structure of the upper ocean. J Phys Oceanogr 34:1949–1966

Foltz GR, Grodsky SA, Carton JA (2004) Seasonal salt budget of the north western tropical Atlantic Ocean along 38°W. J Geophys Res 109:C03052. doi:10.1029/2003JC002111

Fujii Y, Nakaegawa T, Matsumoto S, Yasuda T, Yamanaka G, Kamachi M (2009) Coupled climate simulation by constraining ocean fields in a coupled model with ocean data. J Clim 22:5541–5557

Fujii Y, Kamachi M, Matsumoto S, Ishizaki S (2012) Barrier layer and relevant variability of the salinity field in the equatorial Pacific estimated in an ocean reanalysis experiment. Pure appl Geophys 169(3):579–594

Guinehut S, Dhomps A-L, Larnicol G, Le Traon P-Y (2012) High resolution 3D temperature and salinity fields derived from in situ and satellite observations. Ocean Sci 8:845–857

Hackert E, Ballabrera-Poy J, Busalacchi A, Zhang RH, Murtugudde R (2011) Impact of sea surface salinity assimilation on coupled forecasts in the tropical Pacific. J Geophys Res 116:C05009. doi:10.1029/2010JC006708

Held IM, Soden BJ (2006) Robust responses of the hydrological cycle to global warming. J Clim 19:5686–5699

Hernandez F, Bertino L, Brassington G, Chassignet E, Cummings J, Davidson F, Drévillon M, Garric G, Kamachi M, Lellouche J-M, Mahdon R, Martin MJ, Ratsimandresy A, Regnier C (2009) Validation and intercomparison studies within GODAE. Oceanography 22(3):128–143

Huang B, Xue Y, Behringer DW (2008) Impacts of argo salinity in NCEP global ocean data assimilation system: the tropical Indian Ocean. J Geophys Res 113:C08002. doi:10.1029/2007JC004388

Ingleby B, Huddleston M (2007) Quality control of ocean temperature and salinity profiles—historical and real-time data. J Mar Syst 65:158–175

IPCC (Intergovernmental Panel on Climate Change) (2013) Climate change 2013: the physical science basis. In: Working Group I contribution to the IPCC fifth assessment report. Cambridge University Press, Cambridge, United Kingdom (see www.ipcc.ch/report/ar5/wg1)

Janowiak JE, Bauer P, Wang W, Arkin PA, Gottschalck J (2010) An evaluation of precipitation forecasts from operational models and reanalyses including precipitation variations associated with MJO activity. Mon Weather Rev 138:4542–4560

Johnson ES, Lagerloef GSE, Gunn JT, Bonjean F (2002) Salinity advection in the tropical oceans compared to atmospheric forcing: a trial balance. J Geophys Res 107:8014

Kim J-E, Alexander MJ (2013) Tropical precipitation variability and convectively coupled equatorial waves on submonthly time scales in reanalyses and TRMM. J. Climate 26:3013–3030

Lee T, Awaji T, Balmaseda MA, Greiner E, Stammer D (2009) Ocean state estimation for climate research. Oceanography 22(3):160–167

Levitus S, Antonov JI, Boyer TP, Locarnini RA, Garcia HE, Mishonov AV (2009) Global ocean heat content 1955–2008 in light of recently revealed instrumentation problems. Geophys Res Lett 36:L07608. doi:10.1029/2008GL037155

Levitus S, Antonov JI, Boyer TP, Baranova OK, Garcia HE, Locarnini RA, Mishonov AV, Reagan JR, Seidov D, Yarosh ES, Zweng MM (2012) World ocean heat content and thermosteric sea level change (0–2000 m) 1955–2010. Geophys Res Lett 39:L10603. doi:10.1029/2012GL051106

Maes C, Picaut J, Belamari S (2005) Importance of salinity barrier layer for the buildup of El Niño. J Clim 18:104–118

Maes C, Ando K, Delcroix T, Kessler WS, McPhaden MJ, Roemmich D (2006) Observed correlation of surface salinity, temperature and barrier layer at the eastern edge of the western Pacific warm pool. Geophys Res Lett 33:L06601. doi:10.1029/2005GL024772

Marshall J, Adcroft A, Hill C, Perelman L, Helsey C (1997) A finite-volume, incompressible Navier–Stokes model for studies of the ocean on parallel computers. J Geophys Res 102:5753–5766

Masuda S et al (2010) Simulated rapid warming of Abyssal North Pacific waters. Science 329:319–322

Murtugudde R, Busalacchi AJ (1998) Salinity effects in a tropical ocean model. J Geophys Res 103:3282–3300

O'Kane TJ, Matear RJ, Chamberlain MA, Oke PR (2014) ENSO regimes and the late 1970's climate shift: the role of synoptic weather and South Pacific Ocean spiciness. J Comp Phys 271:19–38

Palmer M, et al (2015) Ocean heat content variability and change in an ensemble of ocean reanalyses. Clim Dyn, pp 1–22. doi:10.1007/s00382-015-2801-0

Rahmstorf S (1996) On the freshwater forcing and transport of the Atlantic thermohaline circulation. Clim Dyn 12:799–811

Santer BD, Wigley TML, Jones PD (1993) Correlation methods in fingerprint detection studies. Clim Dyn 8:265–276

Sprintall J, Wijffels SE, Molcard R, Jaya I (2009) Direct estimates of the Indonesian throughflow entering the Indian Ocean: 2004–2006. J Geophys Res Ocean 114:C07001. doi:10.1029/2008JC005257

Storto A, et al (2015) Steric sea level variability (1993–2010) in an ensemble of ocean reanalyses and objective analyses. Clim Dyn, pp 1–21. doi:10.1007/s00382-015-2554-9

Storto A, Dobricic S, Masina S, Di Pietro P (2011) Assimilating along-track altimetric observations through local hydrostatic adjustments in a global ocean reanalysis system. Mon Weather Rev 139:738–754

Toyoda T, Fujii Y, Yasuda T, Usui N, Iwao T, Kuragano T, Kamachi M (2013) Improved analysis of the seasonal-interannual fields by a global ocean data assimilation system. Theor Appl Mech Japan 61:31–48

Vernieres G, Rienecker MM, Kovach R, Keppenne LC (2012) The GEOS-iODAS: description and evaluation. In: Tech Rep TM-2012-104606, NASA, National Aeronautics and Space Administration Goddard Space Flight Center, Greenbelt, MD

Vialard J, Delecluse P, Menkes C (2002) A modelling study of salinity variability and its effects in the tropical Pacific Ocean during the 1993–1999 period. J Geophys Res 107(C12):8005. doi:10.1029/2000JC000758

Vinje T (2001) Fram Strait ice fluxes and atmospheric circulation, 1950–2000. J Clim 14:3508–3517

von Storch H, Navarra A (1999) Analysis of climate variability: applications of statistical techniques. Springer, Berlin

Vranes K, Gordon AL, Ffield A (2002) The heat transport of the Indonesian throughflow and implications for Indian Ocean heat budget. Deep Sea Res I II 49:1391–1410

Wadley MR, Bigg GR (2006) Are "great salinity anomalies" advective? J Clim 19:1080–1088

Wang X, Chao Y (2004) Simulated sea surface salinity variability in the tropical Pacific. Geophys Res Lett 31:L02302. doi:10.1029/2003GL01

Waters J, Martin M, While J, Lea D, Weaver A, Mirouze I (2014) Implementing a variational data assimilation system in an operational 1/4 degree global ocean model. Q J R Meteorol Soc. doi:10.1002/qj.2388

Xue Y et al (2011) An assessment of oceanic variability in the NCEP climate forecast reanalysis. Clim Dyn 37:2511–2539

Xue Y et al (2012) A comparative analysis of upper-ocean heat content variability from an ensemble of operational ocean reanalyses. J Clim 25:6905–6929

Yang SC, Rienecker M, Keppenne C (2010) The impact of ocean data assimilation on seasonal-to-interannual forecasts: a case study of the 2006 El Niño event. J Clim 23:4080–4095

Yin Y, Alves O, Oke PR (2011) An ensemble ocean data assimilation system for seasonal prediction. Mon Weather Rev 139:786–808

Zhang R, Vallis GK (2006) Impact of great salinity anomalies on the low-frequency variability of the north Atlantic climate. J Clim 19:470–482

Zhang S, Harrison MJ, Rosati A, Wittenberg A (2007) System design and evaluation of coupled ensemble data assimilation for global oceanic studies. Mon Weather Rev 135:3541–3564

Zhao M, Hendon HH, Alves O, Yin Y, Anderson D (2013) Impact of salinity constraints on the simulated mean state and variability in a coupled seasonal forecast model. Mon Weather Rev 141:388–402

Zhao M, Hendon HH, Alves O, Yin Y (2014) Impact of improved assimilation of temperature and salinity for coupled model seasonal forecasts. Clim Dyn 42:2565–2585

Zhu J, Huang B, Balmaseda M (2012) An ensemble estimation of the variability of upper-ocean heat content over the tropical Atlantic Ocean with multi-ocean reanalysis products. Clim Dyn 39:1001–1020

Zhu J, Huang B, Zhang R-H, Hu Z-Z, Kumar A, Balmaseda MA, Marx L, Kinter JL III (2014) Salinity anomaly as a trigger for ENSO events. Nat Sci Rep 4:6821. doi:10.1038/srep06821

Zuo H, Balmaseda MA, Mogensen K (2015) The new eddy-permitting ORAP5 ocean reanalysis: description, evaluation and uncertainties in climate signals. Clim Dyn. doi:10.1007/s00382-015-2675-1